2017

Photoluminescence of Lead Sulfide Quantum Dots of Different Sizes in a Nanoporous Silicate Glass Matrix

Aleksandr P. Litvin

Anton Babaev

Peter Parfenov

See next page for additional authors

Authors

Aleksandr P. Litvin, Anton Babaev, Peter Parfenov, Elena Ushakova, Mikhail Baranov, Olga Andreeva, Kevin Berwick, Anatoly Fedorov, and Alexander Baranov

THE JOURNAL OF PHYSICAL CHEMISTRY C

Article

pubs.acs.org/JPCC

Photoluminescence of Lead Sulfide Quantum Dots of Different Sizes in a Nanoporous Silicate Glass Matrix

Aleksandr P. Litvin,*[,†] Anton A. Babaev,[†] Peter S. Parfenov,[†] Elena V. Ushakova,[†] Mikhail A. Baranov,[†] Olga V. Andreeva,[†] Kevin Berwick,[‡] Anatoly V. Fedorov,[†] and Alexander V. Baranov[†]

[†]ITMO University, Kronverksky pr., 49, St. Petersburg, Russia

[‡]School of Electrical and Electronic Engineering, Dublin Institute of Technology, Kevin Street, Dublin 8, Ireland

ABSTRACT: The optical properties of lead sulfide quantum dots (QDs) of different sizes embedded in a nanoporous silicate glass matrix (NSM) are investigated by steady-state and transient photoluminescence spectroscopy. The use of this matrix allows the fabrication of samples with reproducible optical characteristics, for both isolated and close-packed QDs. Low-temperature PL analysis of isolated QDs with sizes of 3.7 and 4.5 nm shows that the coefficient of temperature shift of the PL position changes sign with reducing QD size because of size-dependent contributions from thermal expansion, mechanical strain, and electron−phonon coupling. The PL intensity is determined by size-dependent splitting of the lowest energy electronic state.

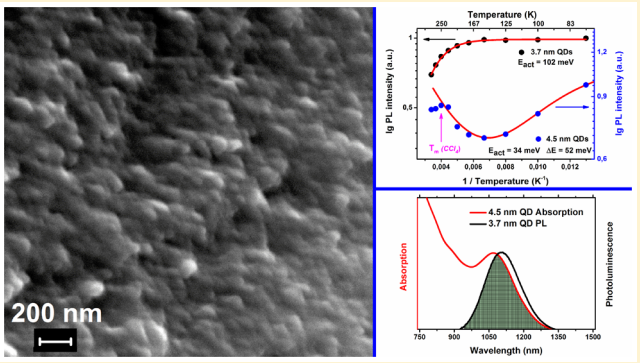

INTRODUCTION

Colloidal quantum dots (QDs) possess a unique ability to control their optical properties by varying their chemical composition, shape, size, and chemical organic ligands.[1] Exploiting this ability should allow a wide range of useful devices to be engineered using these materials. In particular, lead sulfide (PbS) QDs with optical transitions in the near-infrared region are now used in third-generation photovoltaic cells,[2−4] photodetectors,[5−9] and light-emitting diodes.[10−12] However, fundamental research focused on their physical properties remains necessary in order to fully understand the mechanisms governing the relaxation dynamics of QD excitons at the nanoscale.

Identification of a suitable matrix to host these QDs remains an open research question and is crucial for the further development of QD-based devices.[13−18] Any matrix must provide a homogeneous distribution and controllable density of QDs at a relatively high level, optical transparency, and stability of physicochemical properties. Nanoporous silicate glass matrices (NSM) are very promising materials for QD infiltration because they possess excellent optical transmission over a wide spectral range and high radiation and mechanical resistance. Another important advantage of NSMs is that they allow a controlled variation of the pore diameter, opening the possibility of size-selective infiltration of QDs and study of the optical properties of both isolated and close-packed QDs. Several applications of NSMs filled by various nanoparticles such as fullerene-based optical limiters,[19] Ag−AgI-based hybrid "plasmon−exciton" nanostructures,[20] and ammonia vapor sensors[21] have been reported recently.

In this study, we demonstrate that an NSM can be used as a high quality, stable matrix for studying the optical properties of both isolated and close-packed QDs inside the glass pores. While the close-packed regime allows the study of interactions between QDs such as FRET, the opportunity to study isolated QDs in a host matrix allows the examination of the intrinsic properties of the QDs. This allows us to reveal some unusual photoluminescent properties of PbS QDs of different sizes at low temperatures, which are important for a deeper insight into the nature of energy dissipation in lead chalcogenide nanocrystals.

MATERIALS AND EXPERIMENTS

PbS QDs with mean diameters of 3.7 and 4.5 nm, capped by 1.8 nm long oleic acid ligands, have been synthesized by the hot-injection method and dissolved in carbon tetrachloride (CCl_4).[22] The QDs are then embedded into a nanoporous silicate matrix (NSM, with 17 nm pores, made of Na_2O−B_2O_3−SiO_2 glass[19]) and a porous paper matrix (PPM, with micrometer-scale pores, 388 grade Sartorius filter paper[23]).

The samples of NSM with embedded QDs were prepared as follows. Plates of NSM of 1 mm thickness were annealed at 530 °C for 2 h to allow pore purification. Annealing ensures the absence of impurities adsorbed from the air and promotes better penetration of any filling compounds. Next, the NSM plate was placed onto the QD solution/air interface. The concentration of the QDs in the solutions used ranged from

Received: February 28, 2017
Revised: March 24, 2017
Published: March 27, 2017

DOI: 10.1021/acs.jpcc.7b01952
J. Phys. Chem. C 2017, 121, 8645−8652

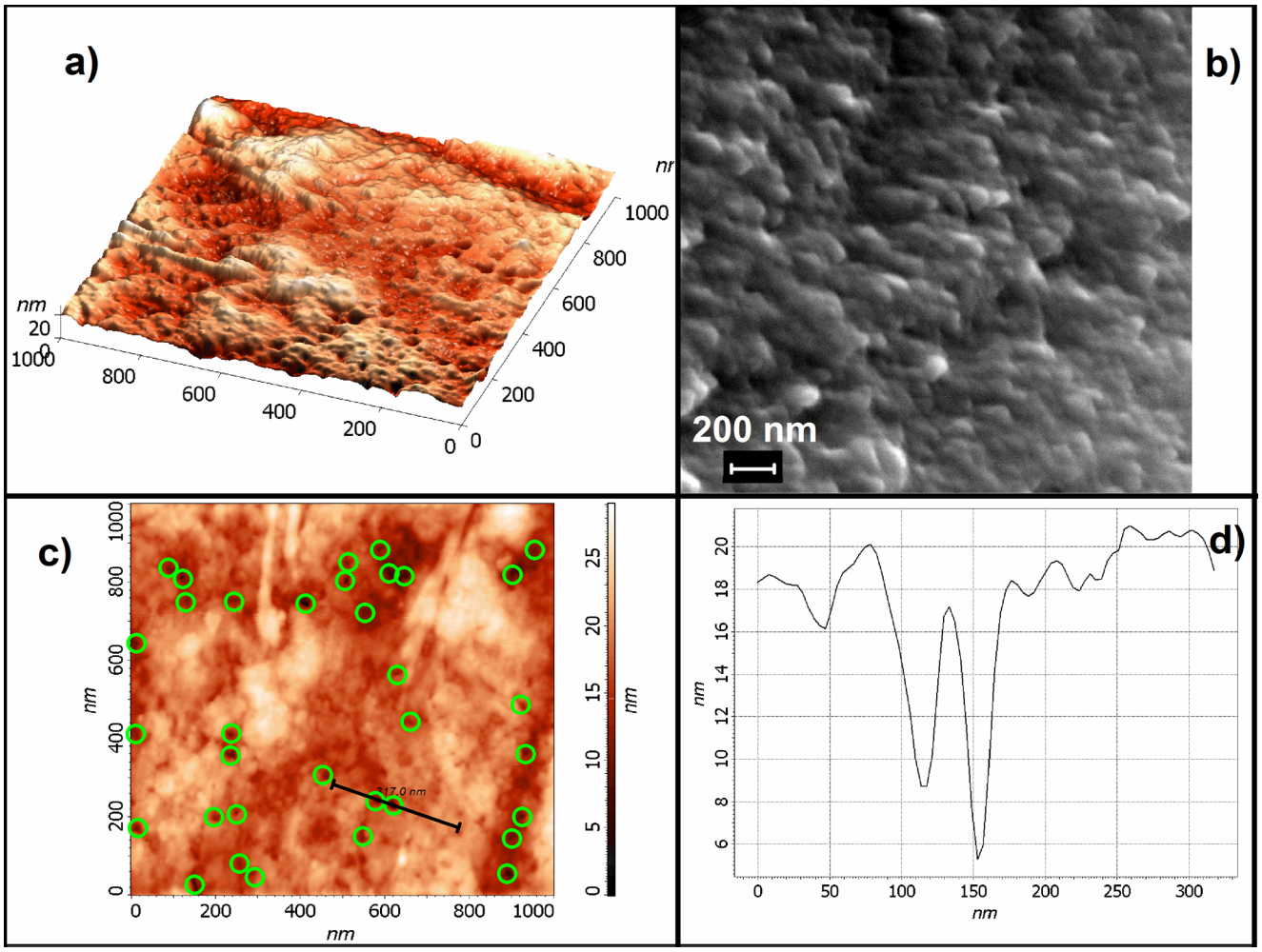

Figure 1. 3D topography of the NSM cross section obtained by AFM (a) and SEM (b). (c) Nanoscale relief of the NSM surface with a few pronounced pores obtained by AFM. (d) The cross section of the NSM surface along the line shown in (c).

10^{-4} to 10^{-5} M, in order to provide different QD concentrations inside the matrix. The solutions were subjected to 30 min of ultrasonication to prevent QD aggregation. After several seconds, the color of the plate becomes light-brown, indicating that the QDs have soaked into the plate. Next, the plate was dipped completely into the colloidal solution to allow homogeneous infiltration of the QDs. To finish, the plate was rinsed several times in CCl_4 solution in order to ensure that the optical responses collected arise from the QDs located inside the NSM volume.

The infiltration and optical properties of QDs in a PPM have been previously investigated in detail.[23] So the samples of the QDs in the PPM were used as a reference. PPM is intended for filtration of residuals with typical sizes larger than 10 μm and is composed of cellulosic fibers with a diameter of a few micrometers, which effectively adsorb semiconductor QDs on their surface.[23] With increasing QD concentration, QDs start to form agglomerates at the fiber surface, and formation of close-packed ensembles of interacting QDs affects their optical properties.[24] Samples of PPM were dipped into CCl_4 colloidal solutions with QD concentrations of $\sim 10^{-5}$ M for 30 s. After that the samples were dried for 1 h at 50 °C to evaporate the residual CCl_4.

Topographic atomic force microscopy (AFM) images of a porous glass surface were obtained by atomic force microscope Solver Pro-M (NT-MDT, Russia) with NSG01 probe (10 nm curvature radii) in semicontact mode. Scanning electron microscopy (SEM) was performed using a Merlin-Zeiss microscope at 15 kV.

The optical properties of the samples were studied using a Shimadzu-UV3600 spectrophotometer and a purpose-built setup for the PL analysis of nanostructures in the NIR.[25] A 633 nm laser excitation was used for steady-state PL analysis, and 532 nm excitation was used for transient measurements. Raw PL spectra were normalized, taking into account the spectral sensitivity of the experimental setup in order to extract the emission spectra.[26]

RESULTS AND DISCUSSION

Nanoporous Silicate Glass Matrix. The surface of the NSM was examined by atomic force and electron microscopies. Figures 1a and 1b demonstrate the 3D topography of the NSM cleavage obtained by AFM and SEM, respectively. The images show nanoscale relief of the NSM. Since the sizes of the pores are close to the probe tip radius, we can distinguish only a few pores on AFM images, as shown in Figure 1c by green circles. The cross section of the NSM surface topography around two closely located pronounced pores is shown in Figure 1d and indicates the pore diameter of ca. 20 nm. The SEM image

DOI: 10.1021/acs.jpcc.7b01952
J. Phys. Chem. C 2017, 121, 8645−8652

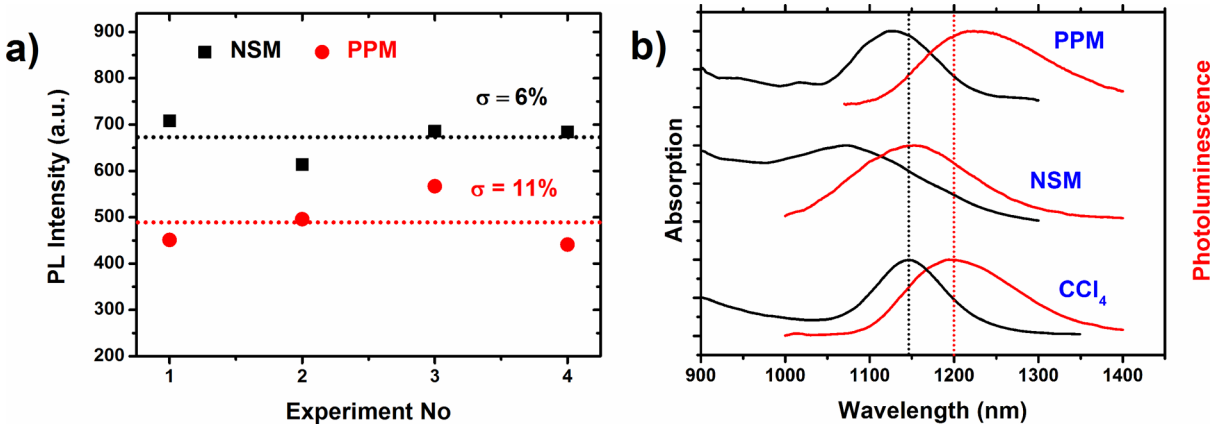

Figure 2. (a) PL peak intensities from four different areas of the porous glass and filter paper with embedded 4.5 nm QDs. (b) Absorption (black lines) and PL (red lines) spectra of 4.5 nm PbS QDs in PPM, NSM, and CCl_4. Vertical dashed lines indicate the centers of the absorption and PL bands for QDs in a CCl_4 colloidal solution.

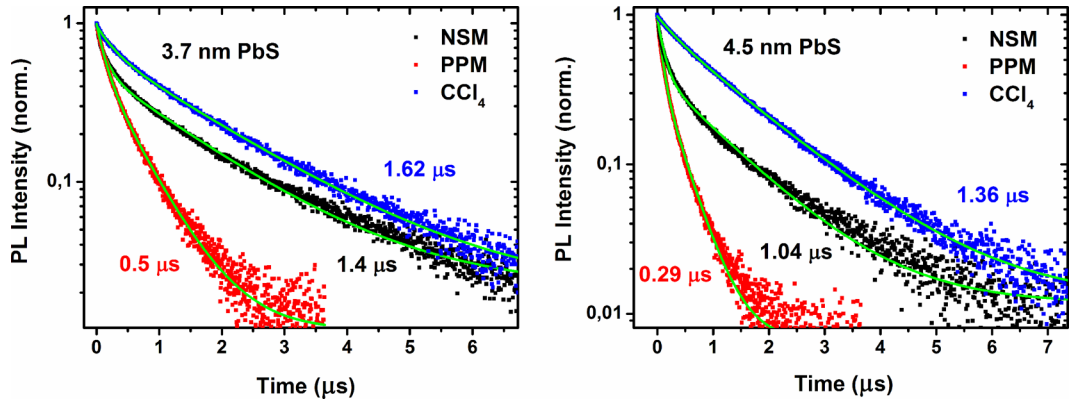

Figure 3. PL decay curves recorded for 3.7 and 4.5 nm PbS QDs in colloidal solution (blue), in porous glass (black), and in filter paper (red). Intensity-weighted average PL lifetimes are shown.

(Figure 1b) shows also pronounced structures with transversal sizes of around 20 nm.

Next, we examined the homogeneity of the spatial QD distribution inside the NSM volume. In order to do this, we compared the optical responses from the NSM sample with those from the PPM samples, which are known to possess homogeneous QD distributions.[23] We chose four different areas on the NSM and PPM samples to record PL spectra. The optical density of the NSM plates at the PL excitation and emission wavelengths was less than 0.1, allowing the examination of the distribution of the QDs inside the sample volume. Results for samples with 4.5 nm PbS QDs are shown in Figure 2a. The black squares and red circles represent the PL peak intensities for the NSM and PPM, respectively. The dotted lines indicate mean values and the standard deviations are listed in the legend. These results demonstrate that we obtained good homogeneity in the QD distribution, in both the NSM and PPM samples. Clearly, the NSM matrix exhibits superior homogeneity in the QD distribution, giving reproducible PL responses.

Noninteracting Regime. Our analysis of the steady-state absorption and PL, as well as the PL decay times, of the NSM filled with QDs shows that a system of noninteracting QDs can be formed inside the NSM. This is supported by Figure 2b, where a comparison between the absorption (black lines) and PL (red lines) spectra of 4.5 nm PbS QDs in PPM, NSM and CCl_4 is shown. The samples of QDs in the NSM and the PPM were obtained by using colloidal solutions with QD concentrations of $\sim 10^{-5}$ M. The absorption bands of the QDs in both the NSM and PPM are blue-shifted compared to those from the QD solution. The magnitude of the shift is dependent on the specific matrix and, in particular, their dielectric constant. The PL band of the PPM sample is red-shifted, indicating FRET is occurring between the QDs.[27] So for PPM we are dealing with close-packed interacting QDs with energy transfer occurring between QDs which differ slightly in size.[24] In contrast, the NSM sample shows no spectral evidence of QD interaction at the QD concentration used, since its PL peak is shifted in the same direction as the absorption peak with an unchanged Stokes shift. It appears that there is a more homogeneous spatial distribution of isolated QDs in the NSM than in the PPM, where conglomerates of close-packed QDs are formed in the pores.

This conclusion is supported by an analysis of the PL decay curves for QDs in CCl_4, NSM, and PPM, performed for 3.7 and 4.5 nm PbS QDs and presented in Figure 3. The PL decay curves obtained for the samples are well fitted by a sum of two exponential functions. We calculated intensity-weighted average PL lifetimes, also shown in Figure 3. Very long decay times for PbS QD colloidal solutions have been previously reported in several papers[22,28−31] and were explained by the contribution of several electronic states to the PL signal.[22,32] To detect interactions between QDs in the different matrices, we performed transient PL analysis with 20 nm spectral selection

DOI: 10.1021/acs.jpcc.7b01952
J. Phys. Chem. C 2017, 121, 8645−8652

inside the luminescence bands of 4.5 nm QDs in CCl_4, NSM, and PPM. The corresponding intensity-weighted average PL lifetimes were calculated for each band and then were normalized by the value, which is the average at the specified spectral range. Spectral dependencies of the normalized intensity-weighted average PL lifetimes are shown in Figure 4. As expected, no notable spectral dependence of PL lifetimes

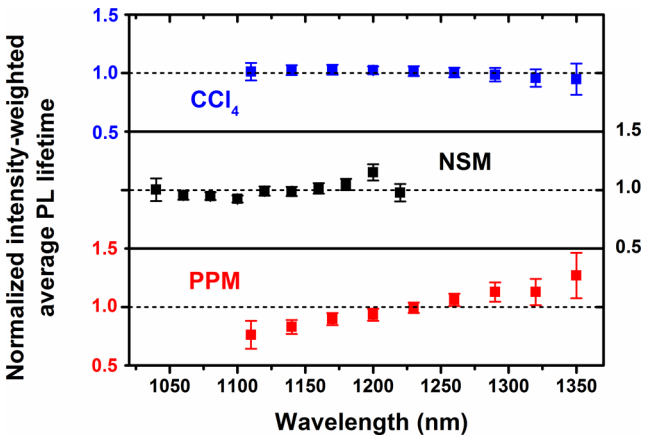

Figure 4. Normalized intensity-weighted average PL lifetimes obtained at different wavelengths for 4.5 nm PbS QDs in colloidal solution (blue), porous glass (black), and filter paper (red).

has been observed for the dilute solution of noninteracting QDs. In contrast, the average PL lifetimes of QDs embedded in the PPM reveal a pronounced wavelength dependence, indicating that quenching of smaller QDs inside a quasi-monodispersed ensemble due to energy transfer[24,27] is taking place. This fact, together with the much shorter PL decay times compared to the QDs in the CCl_4, indicates the formation of conglomerates, composed of strongly interacting QDs. In contrast to the PPM samples, PbS QDs in the NSM demonstrate PL lifetimes with only a slight wavelength dependence. The calculated PL decay times are much closer to those observed in colloidal QD solutions; any slight differences may be ascribed to the difference in the dielectric constant of the matrix or slight optical quenching by the matrix.[33] This observation, together with the minor wavelength dependence of PL lifetimes, shows that the dynamics of energy relaxation for QDs embedded in the NSM are typical of those from isolated QDs. In other words, from an analysis of the absorption and steady-state and transient PL responses of the samples, it is clear that the NSM allows the investigation of the optical properties of individual noninteracting QDs.

Low-Temperature PL Analysis. Since the use of a nanoporous silicate glass matrix allows us to make samples with noninteracting QDs and reproducible optical responses, we were able to explore the PL responses from isolated PbS QDs of different sizes, including the temperature dependencies of PL properties. We performed PL analysis for 3.7 and 4.5 nm PbS QDs embedded in an NSM from colloidal solutions with QD concentrations of 10^{-5} M in the temperature range 77–300 K. Figure 5 represents the temperature dependence of the fwhm of the PL band from the 4.5 nm PbS QDs. The fwhm of the PL band suffers conventional broadening with increasing temperature. The dependence of the fwhm on temperature can be described as follows:[34−36]

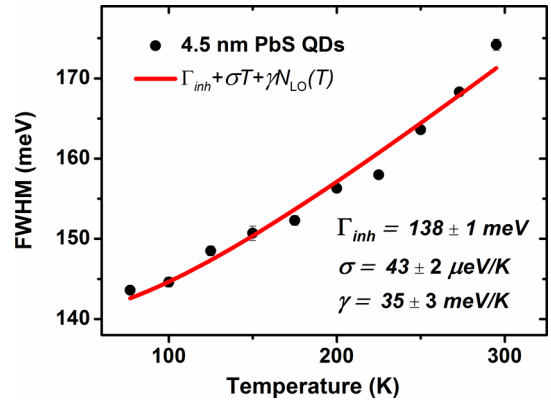

Figure 5. The fwhm temperature dependence for 4.5 nm PbS QDs in NSM. The red line is the fit to the experimental data (solid dots) with eq 1. Fitting parameters are σ = 43 μeV/K, γ = 35 meV/K, and Γ_{inh} = 138 meV, as shown in the legend.

$$\mathrm{fwhm}(T) = \Gamma_{inh} + \sigma T + \gamma\left[\exp\left(\frac{E_{LO}}{k_B T}\right)\right]^{-1} \quad (1)$$

where Γ_{inh} is the QD inhomogeneous distribution width which is temperature-independent, arising mainly from fluctuations in the size and shape of the QDs in the ensemble studied. The coefficients σ and γ are the exciton–acoustic phonon and exciton–LO phonon coupling coefficients respectively, E_{LO} is the LO phonon energy, and k_B is the Boltzmann constant. Fitting the temperature dependence of the fwhm for the 4.5 nm PbS QDs in the NSM by eq 1 with fitting parameters σ, γ, Γ_{inh}, and a fixed value of E_{LO} = 25.4 meV (the bulk value at 296 K[37]) is shown in Figure 5 by the red solid line. Values for σ = 43 μeV/K, γ = 35 meV/K, and Γ_{inh} = 138 meV have been obtained from the fitting procedure. The σ and γ values are close to those reported previously for 5 nm QDs in silicate glass[34] while the Γ_{inh} value is near the width expected at 0 K from a rough extrapolation of the fwhm temperature dependence below 125 K.

Figure 6 represents a temperature dependence of the PL peak position for 3.7 and 4.5 nm PbS QDs embedded in an NSM. The shifts have been approximated by the Varshni equation:[38]

$$E_g(T) = E_{g0} - \alpha\frac{T^2}{T+\beta} \quad (2)$$

where E_{g0} is the bandgap width at 0 K, α is the coefficient of temperature shift of the bandgap energy, and β is the temperature-independent parameter which is usually close to the Debye temperature. An approximation of the PL peak position for 3.7 and 4.5 nm PbS QDs using the Varshni relation with β = 145 K gives coefficients of α of −120 ± 10 and 180 ± 10 μeV/K, respectively, and E_{g0} of 1.178 ± 0.001 and 1.077 ± 0.001 eV, respectively. Olkhovets and co-workers first showed that lead chalcogenide QDs possess a strongly size-dependent temperature coefficient of bandgap energy.[38] They demonstrated that the temperature coefficient of the lowest excited state in the absorption spectra varies over a wide range, from negative values up to the positive value from the bulk material. This is explained by considering the different contributions from thermal expansion, mechanical strain, and electron–phonon coupling, whose size dependencies are especially pronounced for the smallest QDs.

DOI: 10.1021/acs.jpcc.7b01952
J. Phys. Chem. C 2017, 121, 8645–8652

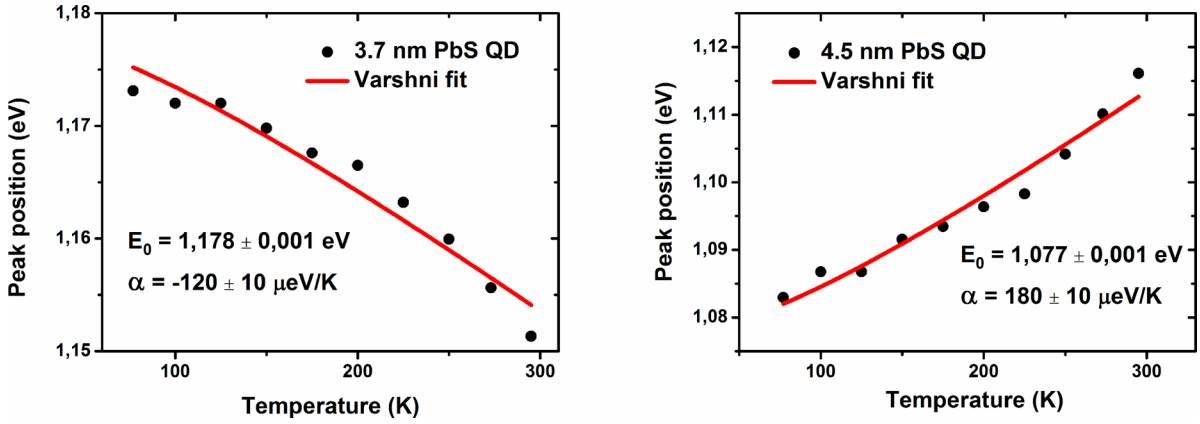

Figure 6. Temperature dependence of the PL peak position for 3.7 and 4.5 nm PbS QDs embedded in the NSM.

This trend was also confirmed in further experiments for lead chalcogenide absorption[39] and PL temperature dependencies.[40] Caram et al. have recently observed different temperature dependencies in the PL position for PbS QDs of different sizes and ascribed this to the redistribution of the state population between two emitting electronic states.[32] In our case, PbS QDs in the NSM did not demonstrate two distinct PL bands, and any variation in the coefficient α should be considered to be a result of the size dependence of various thermal contributions. For 3−4 nm PbS QDs, thermal expansion of the wave function envelope and intraband deformation-potential coupling of electrons to acoustic phonons make a negative contribution to α, leading to a sign change in α.[38]

An analysis of the PL intensity is shown in Figure 7, highlighting another distinction between the luminescent

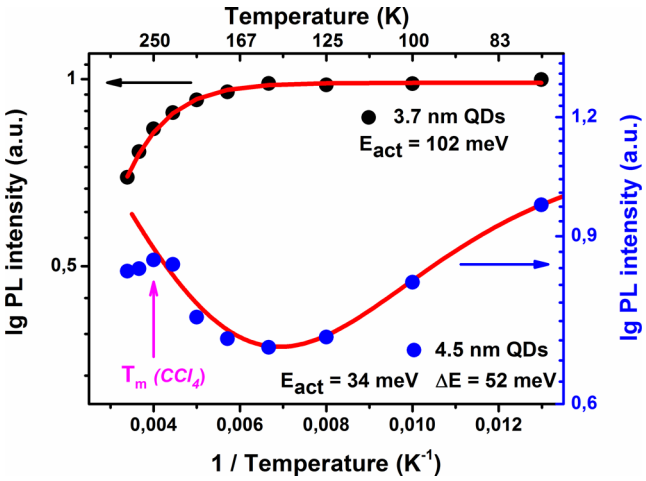

Figure 7. Temperature dependencies of PL intensities for 3.7 and 4.5 nm PbS QDs embedded in an NSM.

properties of 3.7 and 4.5 nm PbS QDs. The temperature dependence of the PL intensity for 3.7 nm QDs is shown by black circles. The dependence for temperatures >60 K can be well fitted by the standard expression (3) with an activation energy E_A:[41]

$$I_{PL} = \frac{I_0}{1 + A \exp\left(-\frac{E_A}{k_B T}\right)} \quad (3)$$

The estimated activation energy of 102 ± 6 meV was found to be close to that for CdTe,[42,43] PbTe,[44] and PbSe/CdSe QDs.[45] Activation energies of 100−130 meV have been recently obtained for PbS QDs from theoretical calculations using a model which includes several emitting states.[32] Zhao et al. have also reported activation energies of 100−130 meV for 3−4 nm PbS QDs capped by oleic acid in PMMA.[40] A relatively slight reduction in the PL intensity with increasing temperature has been previously noted by Turyanska et al. and ascribed to a low density of nonradiative recombination centers.[46]

The temperature dependence of the PL intensity obtained for 4.5 nm PbS QDs is shown in Figure 7 by blue circles and demonstrates a very different behavior. Besides the decrease of PL intensity with decreasing temperature, we observed an unexpected rise in the PL intensity above 150 K. This indicates that at higher temperatures an additional mechanism of radiative recombination is contributing to the PL. It has been shown that PbS QDs possess a complicated low-energy electronic structure, and radiative recombination drastically depends on QD size and temperature.[22,47] Several research groups have reported splitting of the lowest electronic state into "dark" and "bright" states, as shown schematically in Figure 8, assuming the "dark" state can either be highly emissive,[22,31,32] slightly emissive,[34] or nonemissive.[48]

Since the PL band observed in our experiments is highly symmetric for both 3.7 and 4.5 nm QDs in the NSM, we consider a contribution from only one radiative transition from a "bright" state to the total PL signal. However, when the energy gap, ΔE, between "dark" and "bright" states is small enough, thermally activated reverse transitions with a rate constant k_{BD} increase the population of the "bright" state, leading to a growth in the PL signal. This mechanism is illustrated by the red arrow in Figure 8. It is known that energy splitting increases strongly with decreasing QD size;[22,32] thus, this mechanism may be negligible for 3.7 nm QDs.

Taking into account the radiative and nonradiative transitions with the rate constants k_r and k_{nr} and internal conversion to the "dark" state with the rate k_{DB}, the population of the "bright" state N_B will be described by the following equation:

$$\frac{dN_B}{dt} = -(k_r + k_{nr} + k_{DB})N_B + k_{BD}N_D \quad (4)$$

where

DOI: 10.1021/acs.jpcc.7b01952
J. Phys. Chem. C 2017, 121, 8645−8652

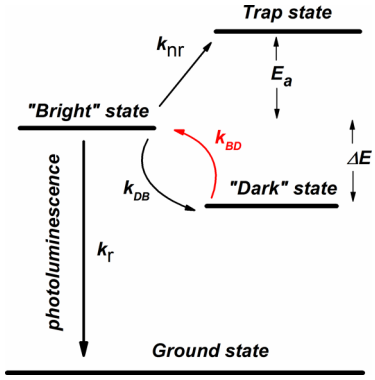

Figure 8. Sketch of the exciton relaxation for the PbS QDs studied. Depopulation of the "bright" state occurs via radiative recombination to the ground state with rate k_r, nonradiative recombination to the trap state separated by activation energy E_a, with rate k_{nr}, and to the "dark" state with rate k_{DB}. Simultaneously, the population of the "bright" state can be increased via thermally activated transitions from the "dark" state at a rate k_{BD}, which depends on the energy gap ΔE between the "dark" and "bright" states.

$$k_{BD} \sim k_{DB} \exp\left(-\frac{\Delta E}{k_B T}\right) \quad (5)$$

Equation 3 can be modified to describe the temperature dependence of the PL intensity for 4.5 nm QDs:

$$I_{PL} = \frac{I_0 + N_D \exp\left(-\frac{\Delta E}{k_B T}\right)}{1 + A \exp\left(-\frac{E_A}{k_B T}\right)} \quad (6)$$

where N_D is a temperature-independent parameter characterizing the population of the "dark" state.[36] Equation 6 is a good fit to the experimental data, as shown in Figure 6, and gives an energy gap, ΔE, between the "dark" and "bright" states, of 52 meV for 4.5 nm QDs, in agreement with data from the literature.[22,47,49] The estimated activation energy E_A for 4.5 nm QDs equals 34 meV.

An additional feature in the PL temperature dependence of 4.5 nm QDs has been observed at 250 K (Figure 7). Since this temperature coincides with the melting point of CCl_4, we speculate that it may be related to the presence of residual solvent within the pores. In our case, upon solvent melting at 250 K, the vibrational modes of liquid CCl_4 become active and further increases in the QD PL intensity may be inhibited by some competing process, such as electronic-to-vibrational energy transfer.[33]

It worth noting that other mechanisms could also lead to changes in the temperature dependence of PL intensity; e.g., the influence of oxygen exposure[50] and FRET[51,52] have also been considered for PbS QDs. However, in our case, the first factor can be excluded since both 3.7 and 4.5 nm QDs would experience similar effects due to oxygen. In addition, FRET is negligible at the low QD concentrations used.

Close-Packed Regime. Besides the opportunity to study optical properties of isolated QDs, the NSM allows the investigation of various interactions at the nanoscale. The NSM is suitable for the experimental study of interactions between semiconductor QDs, plasmonic metal nanoparticles, and biological objects. One example is the Förster resonance energy transfer (FRET) between donor and acceptor nanoparticles.

FRET between two QDs of different sizes exhibits well-known features, allowing an evaluation of the average interdot distance. Since we did not observe any spectral features suggesting QD−QD interaction for the samples prepared from the colloidal solutions with QD concentrations of 10^{-5} M, the QD density in the NSM must be increased. To achieve a higher density in the QD distribution in the NSM matrix, we increased the concentration of the initial QD solution to ~10^{-4} M. We prepared the samples with 3.7 nm QDs, 4.5 nm QDs, and a mixture of 3.7 and 4.5 nm QDs at a 1:1 concentration ratio, keeping the total QD concentration at ~10^{-4} M for all QD solutions. PL spectra for 3.7 nm QDs, 4.5 nm QDs, and their mixture in the NSM are shown in Figure 9a. The spectrum of the QD mixture indicates FRET is taking place between QDs of different sizes, resulting in both quenching of donor PL (3.7 nm QDs) and enhancement of acceptor PL (4.5 nm QDs). Additional evidence for this comes from transient PL analysis. PL decay curves have been recorded at 1000 nm for the samples with a donor-QD and QD mixture and are shown in Figure 9b. At this wavelength, PL from the QD mixture arises from the donor-QDs only and may indicate a quenching process. Indeed, the decay curve for the donor-QDs in the mixture is characterized by a smaller amplitude and shorter PL

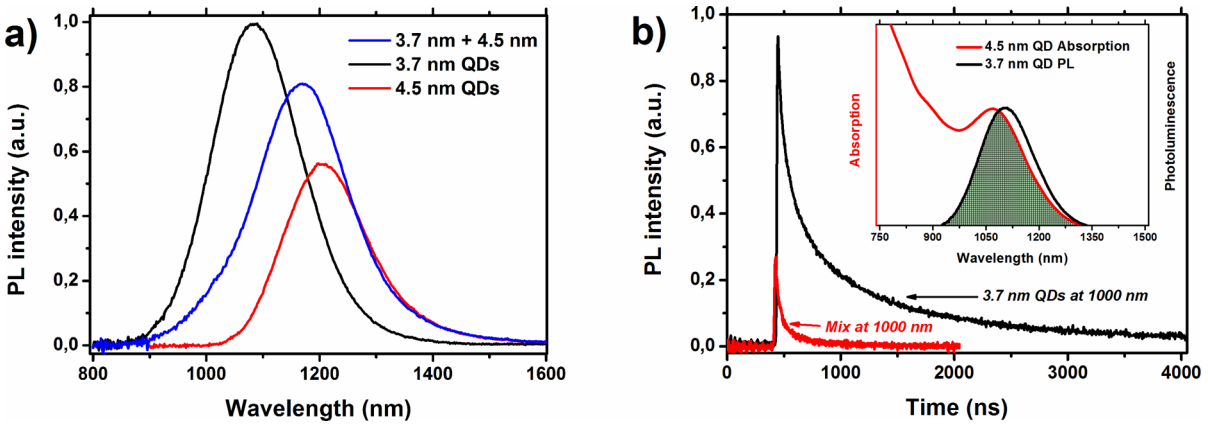

Figure 9. (a) PL spectra for 3.7 nm QDs (black), 4.5 nm QDs (red), and their mixture in NSM (blue). (b) PL decay curves recorded at 1000 nm for the samples with the donor-QD and QD mixture. The inset demonstrates the overlap between the donor PL spectrum and the acceptor absorption spectrum.

DOI: 10.1021/acs.jpcc.7b01952
J. Phys. Chem. C 2017, 121, 8645−8652

lifetime in comparison to the reference sample with 3.7 nm QDs only. This confirms FRET is occurring from the smaller QDs to the larger ones, indicating a short interparticle distance. A FRET efficiency of 74% was extracted from the donor PL lifetimes using the expression[53]

$$E = 1 - \frac{\tau_{DA}}{\tau_D} \quad (7)$$

where τ_{DA} and τ_D are the PL lifetimes of the donor QD in the presence and absence of a QD acceptor, respectively. The Forster radii, which characterize the distance at which energy transfer efficiency equals 50%, can be estimated as follows:[53]

$$R_F^6 = \frac{9000 \ln 10 k^2 Q_D}{128 \pi N_A n^4} \int_0^\infty F_D(\lambda) \varepsilon_A(\lambda) \lambda^4 \, d\lambda \quad (8)$$

where k^2 equals 2/3 and is the orientational factor, the QD-donor quantum yield Q_D is estimated to be ~8% in the NSM, the refractive index n of the NSM with a porosity of 52% with embedded QDs is estimated to be 1.222, and the overlap integral describes the spectral overlap between donor emission and acceptor extinction. R_F equals 8.7 nm, and the corresponding average interdot distance, which can be estimated using the FRET efficiency, equals 7.3 nm. Summation of the calculated interdot distance, oleic acid length, and QDs radii gives a distance close to the diameter of the pores in the NSM, indicating the interaction of two QDs of different sizes in a pore. That correlates well with the equimolar concentration ratio for the sample studied.

CONCLUSIONS

We studied the optical properties of lead sulfide QDs of two different sizes in a nanoporous silicate glass matrix. We showed that the use of a nanoporous glass matrix allowed us to obtain samples with reproducible optical characteristics, both for isolated noninteracting QDs and for QDs forming close-packed structures. Low-temperature PL analysis performed for QDs with sizes of 3.7 and 4.5 nm showed that the coefficient of the temperature shift of PL position changes sign with reducing QD size. This supports a model of size-dependent contributions from thermal expansion, mechanical strain, and electron–phonon coupling to the temperature-induced shift of the lowest energy absorption peak of PbS QDs. Different behaviors of the PL intensity with temperature for QDs of different size was observed and explained by size-dependent splitting of the lowest electronic state and a variation of the energy gap between "dark" and "bright" electronic states.

AUTHOR INFORMATION

Corresponding Author

*(A.P.L.) E-mail: litvin88@gmail.com.

ORCID

Aleksandr P. Litvin: 0000-0001-5261-3210

Notes

The authors declare no competing financial interest.

ACKNOWLEDGMENTS

The authors thank the Ministry of Education and Science of the Russian Federation (State task no. 16.8981.2017/BCh and Grant 14.B25.31.0002) for financial support. A.P.L. thanks the Ministry of Education of the Russian Federation for financial support (scholarship of the President of the Russian Federation for young scientists and graduate students, СП-1841.2015.1)

REFERENCES

(1) Kovalenko, M. V.; Manna, L.; Cabot, A.; Hens, Z.; Talapin, D. V.; Kagan, C. R.; Klimov, V. I.; Rogach, A. L.; Reiss, P.; Milliron, D. J.; et al. Prospects of Nanoscience with Nanocrystals. *ACS Nano* **2015**, *9* (2), 1012−1057.

(2) Carey, G. H.; Abdelhady, A. L.; Ning, Z.; Thon, S. M.; Bakr, O. M.; Sargent, E. H. Colloidal Quantum Dot Solar Cells. *Chem. Rev.* **2015**, *115* (23), 12732−12763.

(3) Duan, J.; Zhang, H.; Tang, Q.; He, B.; Yu, L. Recent Advances in Critical Materials for Quantum Dot-Sensitized Solar Cells: A Review. *J. Mater. Chem. A* **2015**, *3* (34), 17497−17510.

(4) Ning, Z.; Wang, R.; Shang, Y.; Kanjanaboos, P.; Zhou, W.; Sargent, E. H. Colloidal Quantum Dot Ligand Engineering for High Performance Solar Cells. *Energy Environ. Sci.* **2016**, *9* (4), 1130−1143.

(5) Saran, R.; Curry, R. J. Lead Sulphide Nanocrystal Photodetector Technologies. *Nat. Photonics* **2016**, *10* (2), 81−92.

(6) Hu, C.; Gassenq, A.; Justo, Y.; Devloo-Casier, K.; Chen, H.; Detavernier, C.; Hens, Z.; Roelkens, G. Air-Stable Short-Wave Infrared PbS Colloidal Quantum Dot Photoconductors Passivated with Al2O3 Atomic Layer Deposition. *Appl. Phys. Lett.* **2014**, *105* (17), 171110.

(7) Konstantatos, G.; Badioli, M.; Gaudreau, L.; Osmond, J.; Bernechea, M.; Garcia de Arquer, F. P.; Gatti, F.; Koppens, F. H. L. Hybrid Graphene-Quantum Dot Phototransistors with Ultrahigh Gain. *Nat. Nanotechnol.* **2012**, *7* (6), 363−368.

(8) Lee, J. W.; Kim, D. Y.; So, F. Unraveling the Gain Mechanism in High Performance Solution-Processed PbS Infrared PIN Photodiodes. *Adv. Funct. Mater.* **2015**, *25* (8), 1233−1238.

(9) Huang, Y. Q.; Zhu, R. J.; Kang, N.; Du, J.; Xu, H. Q. Photoelectrical Response of Hybrid Graphene-PbS Quantum Dot Devices. *Appl. Phys. Lett.* **2013**, *103* (14), 143119.

(10) Bourdakos, K. N.; Dissanayake, D. M. N. M.; Lutz, T.; Silva, S. R. P.; Curry, R. J. Highly Efficient near-Infrared Hybrid Organic-Inorganic Nanocrystal Electroluminescence Device. *Appl. Phys. Lett.* **2008**, *92* (15), 153311.

(11) Gong, X.; Yang, Z.; Walters, G.; Comin, R.; Ning, Z.; Beauregard, E.; Adinolfi, V.; Voznyy, O.; Sargent, E. H. Highly Efficient Quantum Dot near-Infrared Light-Emitting Diodes. *Nat. Photonics* **2016**, *10* (4), 253−257.

(12) van Veggel, F. C. J. M. Near-Infrared Quantum Dots and Their Delicate Synthesis, Challenging Characterization, and Exciting Potential Applications. *Chem. Mater.* **2014**, *26* (1), 111−122.

(13) He, J.; Wang, Y.; Li, R.; Yuan, X.; Xu, S.; Zhang, L. Tunable and White Light Emitting $AlPO_4$ Mesoporous Glass by Design of Inorganic/organic Luminescent Species. *APL Mater.* **2015**, *3* (4), 046101.

(14) Song, H.; Lee, S. Photoluminescent (CdSe)ZnS Quantum Dot–polymethylmethacrylate Polymer Composite Thin Films in the Visible Spectral Range. *Nanotechnology* **2007**, *18* (5), 055402.

(15) Reda, S. M. Synthesis and Optical Properties of CdS Quantum Dots Embedded in Silica Matrix Thin Films and Their Applications as Luminescent Solar Concentrators. *Acta Mater.* **2008**, *56* (2), 259−264.

(16) Schüler, A.; Python, M.; del Olmo, M. V.; de Chambrier, E. Quantum Dot Containing Nanocomposite Thin Films for Photoluminescent Solar Concentrators. *Sol. Energy* **2007**, *81* (9), 1159−1165.

(17) Jeong, S.; Lee, J.; Nam, J.; Im, K.; Hur, J.; Park, J.-J.; Kim, J.-M.; Chon, B.; Joo, T.; Kim, S. One-Step Preparation of Strongly Luminescent and Highly Loaded CdSe Quantum Dot−Silica Films. *J. Phys. Chem. C* **2010**, *114* (34), 14362−14367.

(18) Solomeshch, O.; Tessler, N. Research Update: Preserving the Photoluminescence Efficiency of near Infrared Emitting Nanocrystals When Embedded in a Polymer Matrix. *APL Mater.* **2016**, *4* (4), 040702.

(19) Andreeva, O. V.; Belousova, I. M.; Veselova, T. V.; Gavronskaya, E. A.; Grigorev, V. A.; Obyknovennay, I. E.; Skobelev, A. G.; Cherkasov, A. S. The Possibility of Using Fullerene-Saturated Porous

DOI: 10.1021/acs.jpcc.7b01952
J. Phys. Chem. C 2017, 121, 8645−8652

Glasses for the Optical Limitation of Laser Radiation. *J. Opt. Technol.* **2001**, *68* (12), 882.
(20) Andreeva, O. V.; Sidorov, A. I.; Stasel'ko, D. I.; Khrushcheva, T. A. Synthesis and Optical Properties of Hybrid "plasmon-Exciton" Nanostructures Based on Ag-AgI in Nanoporous Silica Glass. *Phys. Solid State* **2012**, *54* (6), 1293−1297.
(21) Orlova, A. O.; Gromova, Y. A.; Maslov, V. G.; Andreeva, O. V.; Baranov, A. V.; Fedorov, A. V.; Prudnikau, A. V.; Artemyev, M. V.; Berwick, K. Reversible Photoluminescence Quenching of CdSe/ZnS Quantum Dots Embedded in Porous Glass by Ammonia Vapor. *Nanotechnology* **2013**, *24*, 335701.
(22) Ushakova, E. V.; Litvin, A. P.; Parfenov, P. S.; Fedorov, A. V.; Artemyev, M. V.; Prudnikau, A. V.; Rukhlenko, I. D.; Baranov, A. V. Anomalous Size-Dependent Decay of Low-Energy Luminescence from PbS Quantum Dots in Colloidal Solution. *ACS Nano* **2012**, *6* (10), 8913−8921.
(23) Litvin, A. P.; Parfenov, P. S.; Ushakova, E. V.; Fedorov, A. V.; Artemyev, M. V.; Prudnikau, A. V.; Golubkov, V. V.; Baranov, A. V. PbS Quantum Dots in a Porous Matrix: Optical Characterization. *J. Phys. Chem. C* **2013**, *117* (23), 12318−12324.
(24) Litvin, A. P.; Ushakova, E. V.; Parfenov, P. S.; Fedorov, A. V.; Baranov, A. V. FRET between Close-Packed Quasi-Monodispersed PbS QDs in a Porous Matrix. *J. Phys. Chem. C* **2014**, *118* (12), 6531−6535.
(25) Parfenov, P. S.; Litvin, A. P.; Ushakova, E. V.; Fedorov, A. V.; Baranov, A. V.; Berwick, K. Note: Near Infrared Spectral and Transient Measurements of PbS Quantum Dots Luminescence. *Rev. Sci. Instrum.* **2013**, *84* (11), 116104.
(26) Parfenov, P. S.; Litvin, A. P.; Baranov, A. V.; Veniaminov, A. V.; Ushakova, E. V. Calibration of the Spectral Sensitivity of Instruments for the near Infrared Region. *J. Appl. Spectrosc.* **2011**, *78* (3), 433−439.
(27) Kagan, C.; Murray, C.; Bawendi, M. Long-Range Resonance Transfer of Electronic Excitations in Close-Packed CdSe Quantum-Dot Solids. *Phys. Rev. B: Condens. Matter Mater. Phys.* **1996**, *54* (12), 8633−8643.
(28) Ren, F.; Lindley, S. A.; Zhao, H.; Tan, L.; Gonfa, B. A.; Pu, Y.-C.; Yang, F.; Liu, X.; Vidal, F.; Zhang, J. Z.; et al. Towards Understanding Unusual Photoluminescence Intensity Variation of Ultrasmall Colloidal PbS Quantum Dots with the Formation of Thin CdS Shell. *Phys. Chem. Chem. Phys.* **2016**, *18* (46), 31828.
(29) Clark, S. W.; Harbold, J. M.; Wise, F. W. Resonant Energy Transfer in PbS Quantum Dots. *J. Phys. Chem. C* **2007**, *111* (20), 7302−7305.
(30) Warner, J. H.; Thomsen, E.; Watt, A. R.; Heckenberg, N. R.; Rubinsztein-Dunlop, H. Time-Resolved Photoluminescence Spectroscopy of Ligand-Capped PbS Nanocrystals. *Nanotechnology* **2005**, *16* (2), 175−179.
(31) Fernée, M. J.; Thomsen, E.; Jensen, P.; Rubinsztein-Dunlop, H. Highly Efficient Luminescence from a Hybrid State Found in Strongly Quantum Confined PbS Nanocrystals. *Nanotechnology* **2006**, *17* (4), 956−962.
(32) Caram, J. R.; Bertram, S. N.; Utzat, H.; Hess, W. R.; Carr, J. A.; Bischof, T. S.; Beyler, A. P.; Wilson, M. W. B.; Bawendi, M. G. PbS Nanocrystal Emission Is Governed by Multiple Emissive States. *Nano Lett.* **2016**, *16* (10), 6070−6077.
(33) Aharoni, A.; Oron, D.; Banin, U.; Rabani, E.; Jortner, J. Long-Range Electronic-to-Vibrational Energy Transfer from Nanocrystals to Their Surrounding Matrix Environment. *Phys. Rev. Lett.* **2008**, *100* (5), 57404.
(34) Gaponenko, M. S.; Lutich, A. A.; Tolstik, N. A.; Onushchenko, A. A.; Malyarevich, A. M.; Petrov, E. P.; Yumashev, K. V. Temperature-Dependent Photoluminescence of PbS Quantum Dots in Glass: Evidence of Exciton State Splitting and Carrier Trapping. *Phys. Rev. B: Condens. Matter Mater. Phys.* **2010**, *82* (12), 125320.
(35) Morello, G.; De Giorgi, M.; Kudera, S.; Manna, L.; Cingolani, R.; Anni, M. Temperature and Size Dependence of Nonradiative Relaxation and Exciton-Phonon Coupling in Colloidal CdTe Quantum Dots. *J. Phys. Chem. C* **2007**, *111* (16), 5846−5849.
(36) Jing, P.; Zheng, J.; Ikezawa, M.; Liu, X.; Lv, S.; Kong, X.; Zhao, J.; Masumoto, Y. Temperature-Dependent Photoluminescence of CdSe-Core CdS/CdZnS/ZnS-Multishell Quantum Dots. *J. Phys. Chem. C* **2009**, *113* (31), 13545−13550.
(37) Madelung, O.; Rössler, U.; Schulz, M. Lead Sulfide (PbS) Phonon Dispersion and Frequencies. In *Landolt-Börnstein - Group III Condensed Matter 41C (Non-Tetrahedrally Bonded Elements and Binary Compounds I)*; Springer-Verlag: Berlin, pp 1−3.
(38) Olkhovets, A.; Hsu, R.-C.; Lipovskii, A.; Wise, F. W. Size-Dependent Temperature Variation of the Energy Gap in Lead-Salt Quantum Dots. *Phys. Rev. Lett.* **1998**, *81* (16), 3539−3542.
(39) Dey, P.; Paul, J.; Bylsma, J.; Karaiskaj, D.; Luther, J. M.; Beard, M. C.; Romero, a. H. Origin of the Temperature Dependence of the Band Gap of PbS and PbSe Quantum Dots. *Solid State Commun.* **2013**, *165*, 49−54.
(40) Zhao, H.; Liang, H.; Vidal, F.; Rosei, F.; Vomiero, A.; Ma, D. Size Dependence of Temperature-Related Optical Properties of PbS and PbS/CdS Core/Shell Quantum Dots. *J. Phys. Chem. C* **2014**, *118* (35), 20585−20593.
(41) Krustok, J.; Collan, H.; Hjelt, K. Does the Low-Temperature Arrhenius Plot of the Photoluminescence Intensity in CdTe Point towards an Erroneous Activation Energy? *J. Appl. Phys.* **1997**, *81* (3), 1442−1445.
(42) Stadler, W.; Hofmann, D. M.; Alt, H. C.; Muschik, T.; Meyer, B. K.; Weigel, E.; Müller-Vogt, G.; Salk, M.; Rupp, E.; Benz, K. W. Optical Investigations of Defects in Cd1−xZnxTe. *Phys. Rev. B: Condens. Matter Mater. Phys.* **1995**, *51* (16), 10619−10630.
(43) Krustok, J.; Valdna, V.; Hjelt, K.; Collan, H. Deep Center Luminescence in P-Type CdTe. *J. Appl. Phys.* **1996**, *80* (3), 1757.
(44) Schwarzl, T.; Kaufmann, E.; Springholz, G.; Koike, K.; Hotei, T.; Yano, M.; Heiss, W. Temperature-Dependent Midinfrared Photoluminescence of Epitaxial PbTe/CdTe Quantum Dots and Calculation of the Corresponding Transition Energy. *Phys. Rev. B: Condens. Matter Mater. Phys.* **2008**, *78* (16), 165320.
(45) Abel, K. A.; Qiao, H.; Young, J. F.; van Veggel, F. C. J. M. Four-Fold Enhancement of the Activation Energy for Nonradiative Decay of Excitons in PbSe/CdSe Core/Shell versus PbSe Colloidal Quantum Dots. *J. Phys. Chem. Lett.* **2010**, *1* (15), 2334−2338.
(46) Turyanska, L.; Patané, A.; Henini, M.; Hennequin, B.; Thomas, N. R. Temperature Dependence of the Photoluminescence Emission from Thiol-Capped PbS Quantum Dots. *Appl. Phys. Lett.* **2007**, *90* (10), 101913.
(47) Litvin, A. P.; Parfenov, P. S.; Ushakova, E. V.; Simões Gamboa, A. L.; Fedorov, A. V.; Baranov, A. V. Size and Temperature Dependencies of the Low-Energy Electronic Structure of PbS Quantum Dots. *J. Phys. Chem. C* **2014**, *118* (35), 20721−20726.
(48) Yue, F.; Tomm, J. W.; Kruschke, D. Spontaneous and Stimulated Emission Dynamics of PbS Quantum Dots in a Glass Matrix. *Phys. Rev. B: Condens. Matter Mater. Phys.* **2013**, *87* (19), 195314.
(49) Litvin, A. P.; Parfenov, P. S.; Ushakova, E. V.; Fedorov, A. V.; Artemyev, M. V.; Prudnikau, A. V.; Cherevkov, S. A.; Rukhlenko, I. D.; Baranov, A. V. Size-Dependent Room-Temperature Luminescence Decay from PbS Quantum Dots. *Proc. SPIE* **2012**, *8564*, 85641Z.
(50) Chappell, H. E.; Hughes, B. K.; Beard, M. C.; Nozik, A. J.; Johnson, J. C. Emission Quenching in PbSe Quantum Dot Arrays by Short-Term Air Exposure. *J. Phys. Chem. Lett.* **2011**, *2* (8), 889−893.
(51) Lü, W.; Kamiya, I.; Ichida, M.; Ando, H. Temperature Dependence of Electronic Energy Transfer in PbS Quantum Dot Films. *Appl. Phys. Lett.* **2009**, *95* (8), 083102.
(52) Rinnerbauer, V.; Egelhaaf, H.-J.; Hingerl, K.; Zimmer, P.; Werner, S.; Warming, T.; Hoffmann, A.; Kovalenko, M.; Heiss, W.; Hesser, G.; et al. Energy Transfer in Close-Packed PbS Nanocrystal Films. *Phys. Rev. B: Condens. Matter Mater. Phys.* **2008**, *77* (8), 85322.
(53) Lakowicz, J. R. *Principles of Fluorescence Spectroscopy*; Springer Science & Business Media: 2013.

DOI: 10.1021/acs.jpcc.7b01952
J. Phys. Chem. C 2017, 121, 8645−8652